Supplementary Information for

Distance-dependent regulation of NMDAR nanoscale organization along hippocampal neuron dendrites

Joana S Ferreira[1], Julien P Dupuis, Blanka Kellermayer, Nathan Bénac, Constance Manso, Delphine Bouchet, Florian Levet, Corey Butler, Jean-Baptiste Sibarita, and Laurent Groc[1]

[1]To whom correspondence should be addressed. Emails: laurent.groc@u-bordeaux.fr, joana.ferreira@u-bordeaux.fr

www.pnas.org/cgi/doi/10.1073/pnas.1922477117

This PDF file includes:

Supplementary text: SI Material and methods

Figures S1 to S5

Table S1

SI References

SI Materials and Methods

Primary hippocampal cultures

Hippocampal cultures, containing neurons and glial cells, were prepared from rat at the embryonic stage 18 (E18) and grown on glass coverslips as previously described (1). Briefly, hippocampi were dissected and collected in HBSS containing Penicillin-Streptomycin (PS) and HEPES. Tissues were dissociated with Trypsin-EDTA/PS/HEPES and neurons were plated in Neurobasal medium supplemented with GlutaMAX™ (Gibco, #35050-038) and NeuroCult™ SM1 Neuronal Supplement (Stemcell Technologies, #05711) supplemented with 10% horse serum on coverslips coated with 1 mg/ml poly-L-lysine (PLL) in 60 mm Petri dishes at a density of 275000 to 285000 cells per dish. After 3 to 5 days in culture, the medium was changed for Neurobasal medium/ GlutaMAX™/ NeuroCult™ SM1. One day prior to transfection, half of the culture medium was changed for BrainPhys™ (Stemcell Technologies, #05711) supplemented with NeuroCult™ SM1. Cells were maintained at 36.5°C with 5% CO2. Where indicated, cells were plated to the protocol of Kaech and Banker (2) with minor modifications (3).

DNA constructs

The modified pVIVO2 plasmids expressing the extracellularly YFP-tagged GluN2A (YFP-GluN2A), GluN2B (YFP-GluN2B), and GluN2B subunits with a mutation in the CaMKIIα-binding site (RQHS → QQHD, YFP-GluN2B-RSQD) were previously described (4, 5). Using an In-Fusion strategy following manufacturer instructions (In-Fusion® HD Cloning Kit, # 639650, Takara Bio company), the YFP tag was replaced by an mCherry tag to create the mCherry-GluN2B and mCherry-RSQD constructs. Wild-type CaMKII alpha (GFP-CaMKII) was expressed in the pEGFP-C1 plasmid. Dimeric dsRED-Homer1c (Homer-DsRed) and mcherry-N1 (mCherry) were expressed in the pcDNA3.1 plasmid; SEP-GluA1 [previously used in (6)] was expressed in a pRK5 plasmid.

Transfection

Neurons were transfected at 9-11 days in *vitro* (div) using the calcium-phosphate coprecipitation method (3). For each 18 mm coverslip, 0.5 µg of each DNA construct (YFP-GluN2A, YFP- or mCherry-GluN2B, YFP- or mCherry-GluN2B-RSQD, GFP-CaMKII, SEP-GluA1, mCherry, GFP) plus 0.3 µg of Homer-DsRed (where indicated) were diluted in TE buffer (in mM: 1 Tris–HCl pH 7.3, 1 EDTA). CaCl2 (2.5 M CaCl2 in 10 mM HEPES, pH 7.2) was added to a concentration of 250 mM. This mix was then added dropwise to 2X HEPES-buffered saline (in mM: 12 dextrose, 50 HEPES, 10 KCl, 280 NaCl and 1.5 Na2HPO4·2H2O, pH 7.2). Coverslips containing neurons were transferred to 12-well plates containing 200 µl/well of conditioned culture medium supplemented with 2 mM kynurenic acid (Sigma-Aldrich #K3375). 50 µl of the precipitate solution was added to each well, and incubated for 1-2h at 37 °C. Cells were then washed with unsupplemented Neurobasal medium containing 2 mM kynurenic acid and moved back to their original culture dish. When transfecting NMDAR subunits, 50 µM of D-2-amino-5-phosphonovalerate (D-AP5, Tocris Bioscience, #0106) was added to the culture medium to prevent excitotoxicity. Cells were used 3-4 days after transfection.

Antibodies

Rabbit anti-GluN2A and rabbit anti-GluN2B (custom-made antibodies 2 mg/ml, Agro-Bio, La Ferté Saint Aubin, France) previously described in (3), mouse IgG2a anti-GFP (Thermo Fisher SCIENTIFIC, #A11120), goat anti-mouse Alexa 488 (Thermo Fisher SCIENTIFIC, # A11001), goat anti-mouse Alexa 647 (Thermo Fisher SCIENTIFIC, # 21235) and goat anti-rabbit Alexa 647 (Thermo Fisher SCIENTIFIC, # A21244) were used in this study.

Immunocytochemistry

Live staining was performed as previously described in (3). Where indicated, banker hippocampal neurons (17-18 div) were pre-incubated for 15 min at 37°C with 5 µM of Autocamtide-2-related inhibitory peptide (AIP, Enzo Life Sciences Inc., #ALX-151-029-M001) or

the respective control peptide (TAT-NS). For neuronal activity blokade experiments, cells were pre-incubated for 1h with 1 µm of tetrodotoxin (TTX, #1069, TOCRIS) or buffer only (basal) before immunostaining. TTX was maintained during live-staining. Hippocampal neurons (9-15 div), expressing soluble GFP, were surface live-immunostained for endogenous GluN2A-NMDAR or GluN2B-NMDAR using custom-made anti-GluN2A or anti-GluN2B antibodies, respectively (0.1 mg/ml). Transfected neurons, with GluN2A-, GluN2B- (wild-type or mutant) and CaMKII, were stained at 13-15 div with anti-GFP antibodies (1:1000) for 15 min at 37°C. Cells were fixed for 15 min in 4% paraformaldehyde (Sigma-Aldrich, #P6148)/4% sucrose (Sigma-Aldrich, #0389) in PBS (Euromedex, #ET330) at room temperature (RT), then incubated for 1h with a blocking solution containing 1.5% bovine serum albumin (BSA, Sigma-Aldrich, #A3059)/0.1% fish skin gelatin (Sigma-Aldrich, #G7765)/0.1% Triton X-100 (Sigma-Aldrich, #T9284). For intracellular staining, primary antibodies were added after fixation and a 5 min permeabilization step with 0.4% Triton X-100/PBS solution. The secondary antibodies (0.1mg/ml concentration) were prepared in blocking solution and incubated for 1h at room temperature, after what a second fixation was performed. Between incubation steps, cells were washed with PBS supplemented with 50 mM NH_4Cl (Sigma-Aldrich, #A4514). Cells were kept in PBS at 4°C until imaging.

dSTORM imaging

Imaging sessions were performed either on a Nikon Ti Eclipse (Nikon France S.A.S., Champigny-sur-Marne, France) system or on a commercial Leica SR GSD microscope (Leica Microsystems, Wetzlar, Germany).

The Nikon Ti Eclipse system was equipped with a Perfect Focus System (PFS), an azymuthal Ilas² TIRF arm (Gataca Systems, Massy, France) and an Apo TIRF 100 X oil-immersion objective (NA 1.49) and an Evolve EMCCD camera (Photometrics, Tucson, USA) with a final pixel size of 160nm. Acquisitions were performed with an Ilas² scanner system (Gataca Systems, Massy, France) and

a 635 nm diode laser. A 405 nm diode laser was used to keep an optimal number of stochastically activated molecules per frame. This system was equipped with a Ti-S-ER motorized stage controlled by MetaMorph software (Molecular Devices, Sunnyvale, USA). Samples were illuminated in TIRF mode and images were obtained with an exposure time of 20 ms with up to 80,000 consecutive frames. Imaging was carried out at room temperature in a closed Ludin chamber (Life Imaging Services, Switzerland) using a pH-adjusted extracellular solution containing oxygen scavengers and reducing agents (7, 8). Single-molecule localization and reconstruction was performed online with automatic feedback control of the lasers using the WaveTracer module, enabling optimal single-molecule density during the acquisition (9). The acquisition and localization sequences were driven by MetaMorph software in a streaming mode at 50 frames per second (20 ms exposure time) using a region of interest of 256x256 pixels and a pixel size of 160 nm. Super-resolution images were reconstructed with the PALMTracer software plugin for MetaMorph using a Gaussian fit (xy sigma) to determine the centroid-coordinates of a single molecule and lateral drift correction, using multicolor fluorescent microspheres (#T7279 TetraSpeck, Life Technologies).

The Leica SR GSD microscope was equipped with a Leica HC PL Apo TIRF 160x oil-immersion objective (NA 1.43) enabling detection of single fluorophores and an EMCCD iXon camera (ANDOR, Belfast, UK) with a final pixel size of 100 nm. Samples were illuminated in TIRF mode and images were obtained with an exposure time of 10.85 ms with up to 100,000 consecutive frames. Imaging was carried out at room temperature in a closed Ludin chamber (Life Imaging Services, Switzerland) using a pH-adjusted extracellular solution containing oxygen scavengers (Pyranose oxidase) and reducing agents (10). Image acquisition was controlled by the Leica LAS software. First, the ensemble fluorescence of Alexa 647 was converted into dark state using 50% of full power of the 642 nm laser (500 mW). Once the desired number of single fluorophores per

frame was reached, the intensity of the 642 nm laser was reduced to 15% of full laser power. In order to keep an optimal number of stochastically activated molecules per frame, the power of the 642 nm laser was increased up to a maximum of 25% and/or the 405 nm laser (30 mW) was continuously adjusted, reaching no more than 10% of full laser power. The particle detection threshold was set to 20 in the Leica LAS software. Super resolution images were reconstructed by the Leica LAS software using a fitting algorithm determining the centroid-coordinates of a single molecule and fitting the point-spread-function (PSF) of a distinct diffraction limited event to a Gaussian function. The generated super-resolved images had a final spatial resolution of 40 nm. Multicolor fluorescent microspheres (#T7279 TetraSpeck, Life Technologies) were used for lateral drift correction.

We used the SR-Tesseler software (10) to quantify protein clustering from the localized molecule coordinates. This method uses a Voronoi diagram to decompose a super-resolution image into polygons of various sizes centered on the localized molecules. From those polygons, several parameters can be extracted such as the first-rank density σ_i^1 (10) of a molecule *i*. Automatic segmentation of clusters was performed by keeping molecules having a density σ_i^1 higher than $2\sigma^d$, with σ^d the average density of the dataset. All selected neighboring molecules were merged and we only kept clusters having a minimum area of 1.25 (NMDAR) or 0.94 (CaMKII) px^2 and a minimum number of localizations of 5. The parameters used to define CaMKII clusters segmentation in SR-Tesseler analysis software were based on rotary shadow electron microscopy studies reporting an average CaMKII cluster diameter of 100 nm (11), parameters to define NMDAR clusters were previously defined in (3). For each cluster *j*, automatic segmentation of the nanodomains was achieved by applying $\sigma_{i,j}^1 > 1\sigma_j^o$, with σ_j^o the average density of the cluster *j* and $\sigma_{i,j}^1$ the density of its i^{th} molecule. Similarly to the clusters, all selected neighboring molecules were merged and we only kept nanodomains having a minimum

area of 0.006 (NMDAR) or 0.22 (CaMKII) px^2 and a minimum number of localizations of 25. Nanodomain segmentation parameters were defined based on single particle electron microscopy studies describing the CaMKII holoenzyme complex as having a 35 nm maximum diameter (12), NMDAR nanodomains segmentation parameters details can be found in (3). Size parameters of both the clusters and the nanodomains were extracted by principal component analysis. Local densities were calculated as the number of localizations divided by the respective area of the cluster or nanodomain in $pixel^2$ (px^2).

Epi-fluorescence image acquisition and analysis

Wild-type and mutant GFP-CaMKII epifluorescence images were obtained on a Nikon Ti Eclipse equipped with a Plan Fluor Apo 40X oil-immersion objective (NA 1.3), a Perfect Focus System (PFS), a SOLA light engine (Lumencor, Beaverton, USA) illumination system, proper excitation and emission filters (Sutter Intrument), and a sensitive Evolve EMCCD camera. This system was controlled by MetaMorph software. All other epi-fluorescence images were obtained on the optical system described above, before the start of dSTORM imaging sessions.

All epi-fluorescence images analysis was performed in ImageJ 1.52n (National Institutes of Health, USA). For Homer-DsRed or Homer-GFP area analysis, images were subjected to an algorithm-based automatic threshold (13) and dendritic spines were defined as regions of interest. For NMDAR cluster analysis, a user-defined intensity threshold was used for cluster selection and background subtraction. The number of clusters was measured for all selected regions and normalized to the dendrite length. Integrated density of wild-type or mutant CaMKII was obtained by measuring the mean GFP fluorescence intensity within dendritic spines. Regions of interest were adjusted according to the spine size.

Single Quantum Dot tracking

Cultured hippocampal neurons at 14-15 div were first incubated for 10 min with rabbit anti-GFP polyclonal antibodies (#A-6455, Thermo Fisher Scientific Inc., Cambridge, United Kingdom, 1:50000), washed and then incubated for 10 min with F(ab')2-Goat anti-Rabbit IgG (H+L) Secondary Antibody, Qdot 655 (#Q11422MP, Thermo Fisher Scientific Inc., Cambridge, United Kingdom, 1:50000). All incubations were done in pre-heated Tyrode solution (in mM: 105 NaCl, 5 KCl, 2 $MgCl_2$, 2 $CaCl_2$, 12 D-glucose, 25 HEPES, pH 7.4) supplemented with 1% BSA. QD were detected by using a mercury lamp and appropriate excitation/emission filters. Images were obtained with an acquisition time of 50 ms (20 Hz) with up to 500 consecutive frames. Signals were detected using an EMCCD camera (EvolveTM, Photometrics). QD recording sessions, which lasted up to 20-25 min, were processed with the Metamorph software. The instantaneous diffusion coefficient 'D' was calculated for each trajectory, from linear fits of the first 4 points of the mean-square-displacement versus time function using MSD(t) = <r2> (t) = 4Dt. The two-dimensional trajectories of single molecules in the plane of focus were constructed by correlation analysis between consecutive images using a Vogel algorithm. This technique provides with a high accuracy of single QD detection (~30 nm resolution) which we used to measure the dynamic distribution of YFP-GluN2B-NMDAR, YFP-GluN2A-NMDAR or YFP-GluN2B-RSQD at synaptic sites. Synaptic areas were defined using transfected Homer-DsRed as a marker.

One-photon glutamate-uncaging and analysis

Imaging sessions were performed on a Nikon Ti Eclipse microscope (see details in the dSTORM imaging section). All acquisitions were performed at 37°C and piloted using the Metamorph software. Hippocampal neurons were co-transfected at 10-11 div with SEP-GluA1 and Homer-DsRed, wild-type mCherry-GluN2B or mCherry-GluN2B-RSQD, a mutant that is deficient for binding to CaMKII. Co-transfection with mCherry-GluN2B or mCherry-GluN2B-RSQD was visually

confirmed before acquisition. Neurons were imaged at 14-15 div in magnesium-free HEPES-Tyrode (in mM: 110 NaCl, 5 KCl, 2 $CaCl_2$, 15 Glucose, 25 HEPES, pH 7.4) supplemented with TTX (1 µM) to avoid hyper-activation. For glutamate uncaging, 2 mM of MNI-caged-L-glutamate (#1490, TOCRIS) were added directly into the imaging chamber, alone or in combination with 50 µM AP5 (D-AP5, #0106, TOCRIS) and 10 µM NBQX (#0373, TOCRIS) to block glutamatergic receptor-mediated activity, where indicated. SEP-GluA1 fluorescence was imaged before and after uncaging using a 491 nm wavelength laser, and 1-photon glutamate uncaging was achieved with a 405 nm wavelength laser (20 repetitions, 0.5 Hz), using the Ilas² scanner system (Gataca Systems, Massy, France).On average, 10 to 15 spines per dendritic region were randomly selected based on their morphology. 20 min after uncaging, the same region of interest was acquired using identical laser power and acquisition time as before uncaging.

The mean intensity of SEP-GluA1 fluorescence in 10 x 10 pixels regions of interest around the uncaged area was measured before and after uncaging, using ImageJ. Only spines presenting a minimum 1.4-fold increase in SEP-GluA1 fluorescence intensity after uncaging (i.e. above the standard deviation of SEP-GluA1 fluorescence intensity in our experimental conditions) were considered as potentiated to rule out intrinsic intensity variations. The efficacy of potentiation was calculated as the number of potentiated spines divided by the total number of uncaged spines. As a validation, this efficacy was monitored either (i) in the absence of caged MNI-glutamate, (ii) in the presence of caged MNI-glutamate alone and (iii) in the presence of caged MNI-glutamate plus glutamate receptors antagonists (AP5 and NBQX) in order to rule out modifications strictly resulting from laser pulses and to ensure the glutamate receptor-dependence of LTP induction, respectively.

Statistical analysis

Statistical analysis was performed with the help of GraphPad Prism 8.2.1 software. Details concerning *n* values, number of independent experiments, statistical tests used and exact *P* values can be found in SI Appendix, Table S1.

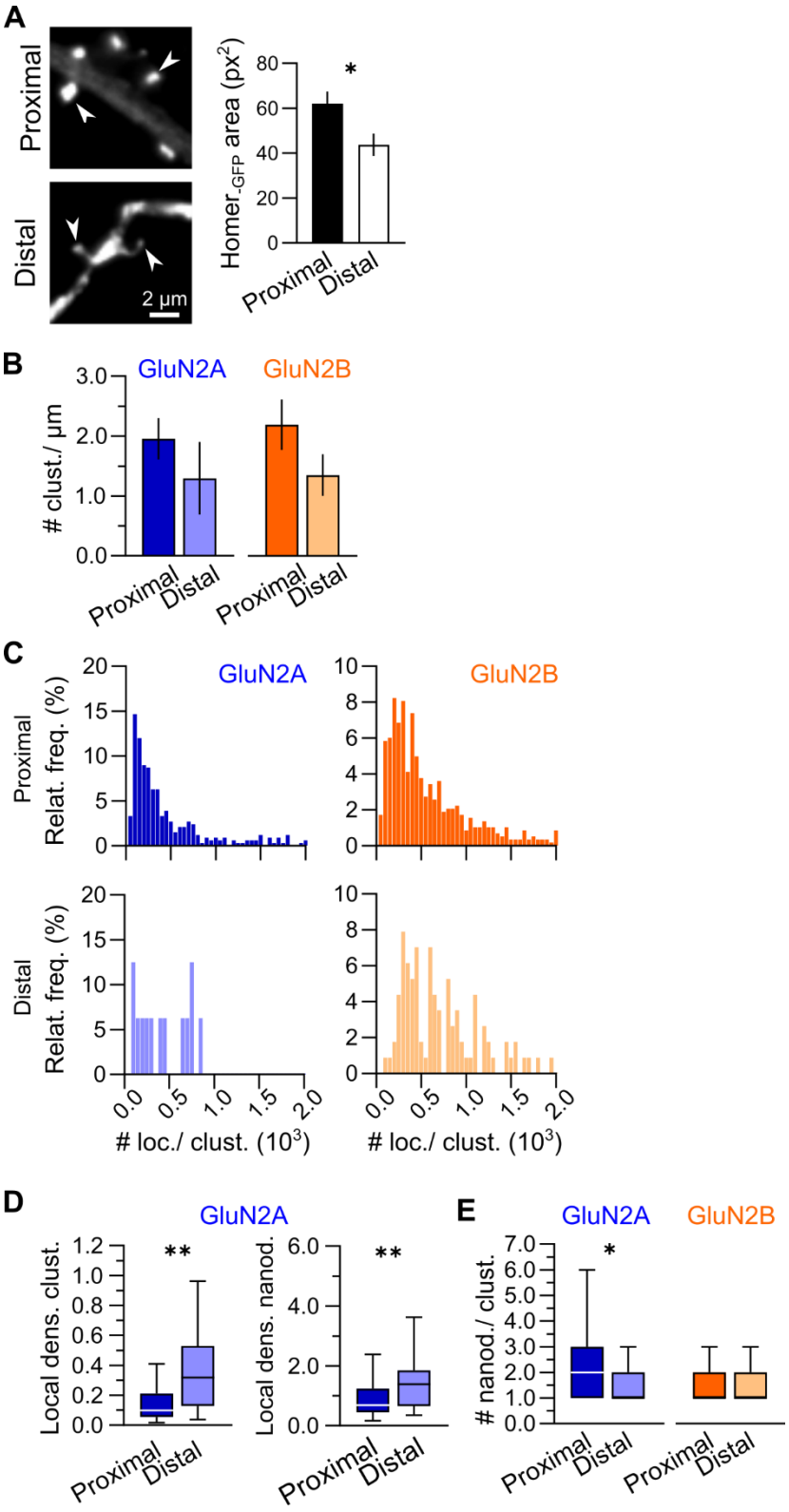
A
Proximal
Distal
2 µm
Homer-GFP area (px²)
80
60
40
20
0
*
Proximal
Distal
B
GluN2A
GluN2B
clust./ µm
3.0
2.0
1.0
0.0
Proximal
Distal
Proximal
Distal
C
GluN2A
GluN2B
Proximal
Relat. freq. (%)
Distal
Relat. freq. (%)
loc./ clust. (10³)
loc./ clust. (10³)
D
GluN2A
Local dens. clust.
**
Local dens. nanod.
**
Proximal
Distal
Proximal
Distal
E
GluN2A
GluN2B
nanod./ clust.
*
Proximal
Distal
Proximal
Distal

Fig. S1. GluN2A- and GluN2B-NMDAR dSTORM imaging. (*A*) Proximal (*top; left*) and distal (*bottom; left*) dendritic portions of hippocampal neurons transfected with Homer-GFP. Spine size was evaluated based on Homer-GFP cluster area (*right*). (*B*) Proximal (*dark colors*) and distal (*light colors*) linear densities (number of clusters per dendritic length; # clust./ µm) of GluN2A-NMDAR (*blue*) and GluN2B-NMDAR (*orange*). Data are presented as mean ± SEM. (*C*) Relative frequency distributions (Relat. freq.) of GluN2A-NMDAR (*blue*) and GluN2B-NMDAR (*orange*) number of localizations per cluster (# loc./ clust.) at proximal (*dark colors*) and distal (*light colors*) dendritic segments. *(D)* Local densities of proximal and distal GluN2B-NMDAR clusters (Local dens. clust.; *left*) and nanodomains (Local dens. nanod.; *right*). *(E)* Proximal (*dark colors*) and distal (*light colors*) number of GluN2A-NMDAR (*blue*) and GluN2B-NMDAR (*orange*) nanodomains per cluster (#nanod./ clust.). Data are represented as box and whisker plots: line at median, IQR box, whiskers minimum and maximum values. * $P \leq 0.05$; ** $P \leq 0.01$; no symbol $P > 0.05$. For statistical details refer to *SI Appendix, Table S1*.

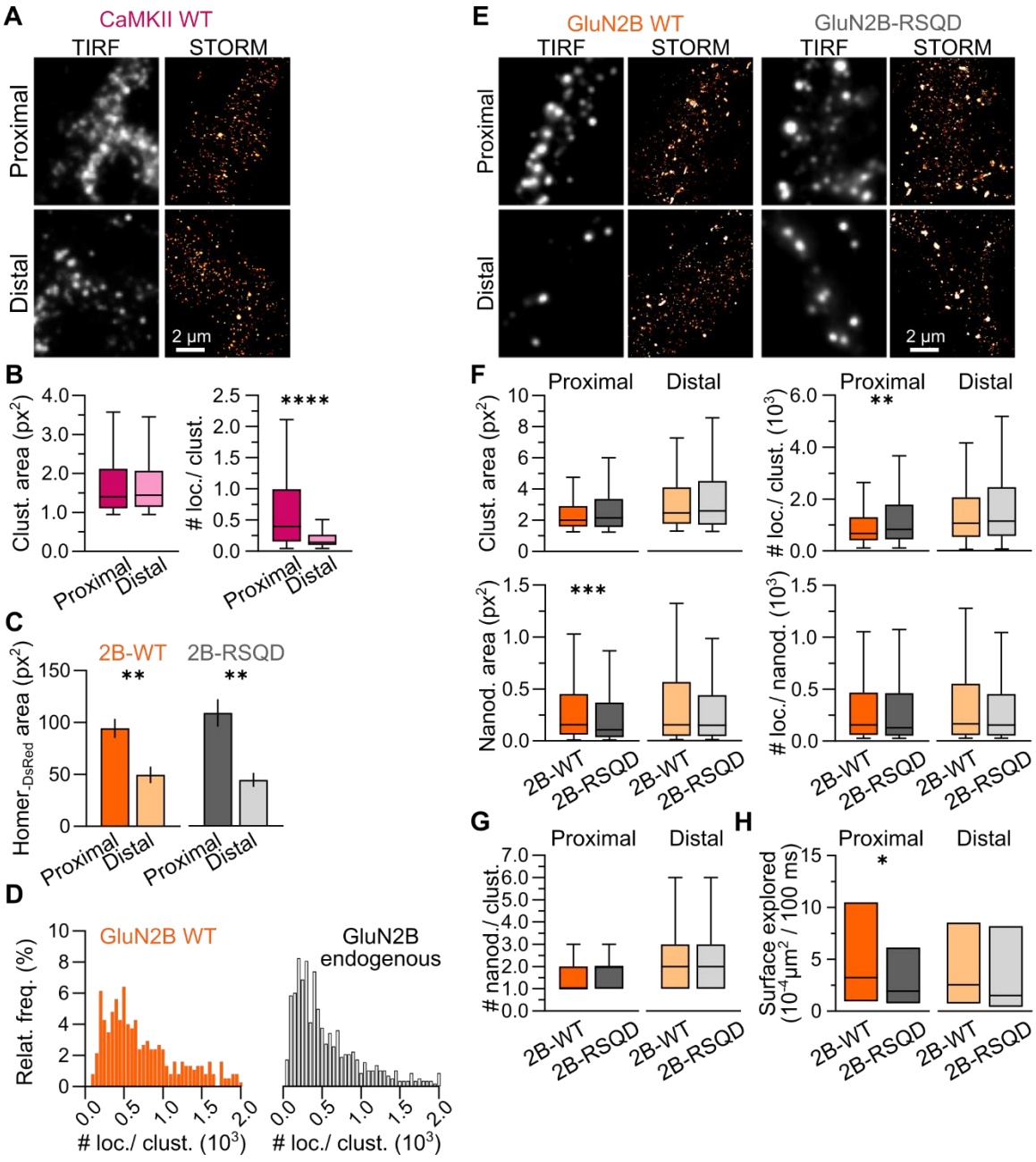

Fig. S2. Interaction with CaMKII regulates the nano-organization of GluN2B-NMDAR. (*A*) Representative low resolution (TIRF, *black and while panels*) and high resolution (dSTORM; *gold pseudo-color panels*) images of wild-type GFP-CaMKII at proximal (*CaMKII WT; top*) or distal (*bottom*) dendritic segments. (*B*) Cluster areas (Clust. area; *left*) and number of localizations per cluster (# loc./ clust.; *right*) of wild-type GFP-CaMKII at proximal (*dark colors*) and distal (*light*

colors) segments. Data are represented as box and whisker plots: line at median, IQR box, whiskers minimum and maximum values. (*C*) Proximal (*dark colors*) and distal (*light colors*) Homer-DsRed cluster areas of neurons transfected with wild-type YFP-GluN2B (*2B-WT; orange*) or mutant YFP-GluN2B-RSQD (*2B-RSQD; gray*). Data are presented as mean ± SEM. (*D*) Relative frequency distributions (Relat. Freq.) of YFP-GluN2B-NMDAR (*GluN2B WT; orange*) and endogenous GluN2B-NMDAR (*white*) number of localizations per cluster (# loc./ clust.) at proximal dendritic segments. (*E*) Representative low resolution images of wild-type YFP-GluN2B (*GluN2B WT*; *left*) or mutant YFP-GluN2B-RSQD (*GluN2B-RSQD*; *right*) acquired in total internal reflection fluorescence (TIRF) microscopy (*black and white panels*) from proximal (*top*) or distal (*bottom*) dendritic segments, and the corresponding high resolution images obtained by dSTORM (*gold pseudo-color panels*). *(F)* Cluster areas (Clust. area; *top left*), number of localizations per cluster (# loc./ clust.; *top right*), nanodomain areas (Nanod. area; *bottom left*) and number of localizations per nanodomain (# loc./ nanod.; *bottom right*) of wild-type YFP-GluN2B (*2B-WT*; *orange*) or mutant YFP-GluN2B-RSQD (*2B-RSQD; gray*) at proximal (*dark colors*) or distal (*light colors*) segments. *(G)* Number of wild-type YFP-GluN2B (*2B-WT*) or mutant YFP-GluN2B-RSQD (*2B-RSQD*) nanodomains per cluster (#nanod./ clust.) at proximal (*left*) or distal (*right*) locations. Data are represented as box and whisker plots: line at median, IQR box, whiskers minimum and maximum values. (*E*) Surface explored by wild-type YFP-GluN2B (*2B-WT; orange*) and YFP-GluN2B-RSQD *(2B-RSQD; gray*) at proximal (*dark colors*) or distal (*light colors*) dendritic segments. Data are represented as median ± IQR. * $P \leq 0.05$; ** $P \leq 0.01$; *** $P \leq 0.001$; **** $P \leq 0.0001$; no symbol $P > 0.05$. For statistical details refer to *SI Appendix, Table S1*.

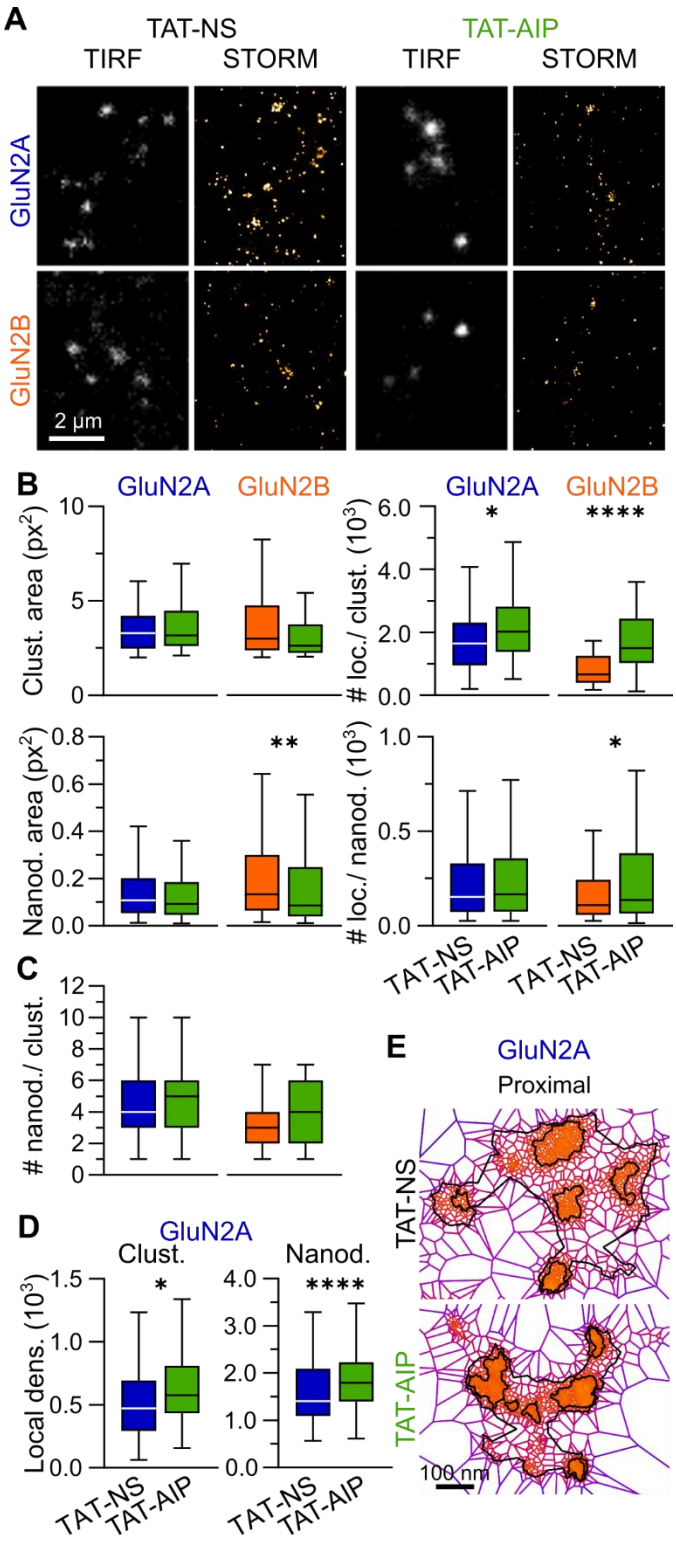

Fig. S3. CaMKII activity regulates the nano-organization of GluN2B-NMDAR at proximal locations. (*A*) Representative low resolution (TIRF) and super-resolved (dSTORM) images of

GluN2A-NMDAR (*top*) and GluN2B-NMDAR (*bottom*) at proximal locations after incubation with a control peptide (*TAT-NS; left*) or a CaMKII inhibiting peptide (*TAT-AIP; right*). *(B)* Cluster areas (Clust. area; *top left*), number of localizations per cluster (# loc./ clust.; *top right*), nanodomain areas (Nanod. area; *bottom left*) and number of localizations per nanodomain (# loc./ nanod.; *bottom right*) of GluN2A- (*blue*) and GluN2B-NMDAR (*orange*) at proximal locations after treatment with TAT-NS (*dark colors*) or TAT-AIP (*green*) peptides. *(C)* Number of nanodomains per cluster (#nanod./ clust.) of GluN2A- (*blue*) and GluN2B-NMDAR (*orange*) at proximal locations after treatment with TAT-NS (*dark colors*) or TAT-AIP (*green*). *(D)* Local densities (Local dens.) of GluN2A-NMDAR clusters (*left*) and nanodomains (*right*) after treatment with TAT-NS (*dark blue*) or TAT-AIP (*green*). Data are represented as box and whisker plots: line at median, IQR box, whiskers minimum and maximum values. * $P \leq 0.05$; ** $P \leq 0.01$; **** $P \leq 0.0001$; no symbol $P > 0.05$. For statistical details refer to *SI Appendix, Table S1*. (*E*) Representative GluN2A-NMDAR clusters after incubation with TAT-NS (*top*) or TAT-AIP (*bottom*) peptides obtained with SR Tesseler software analysis.

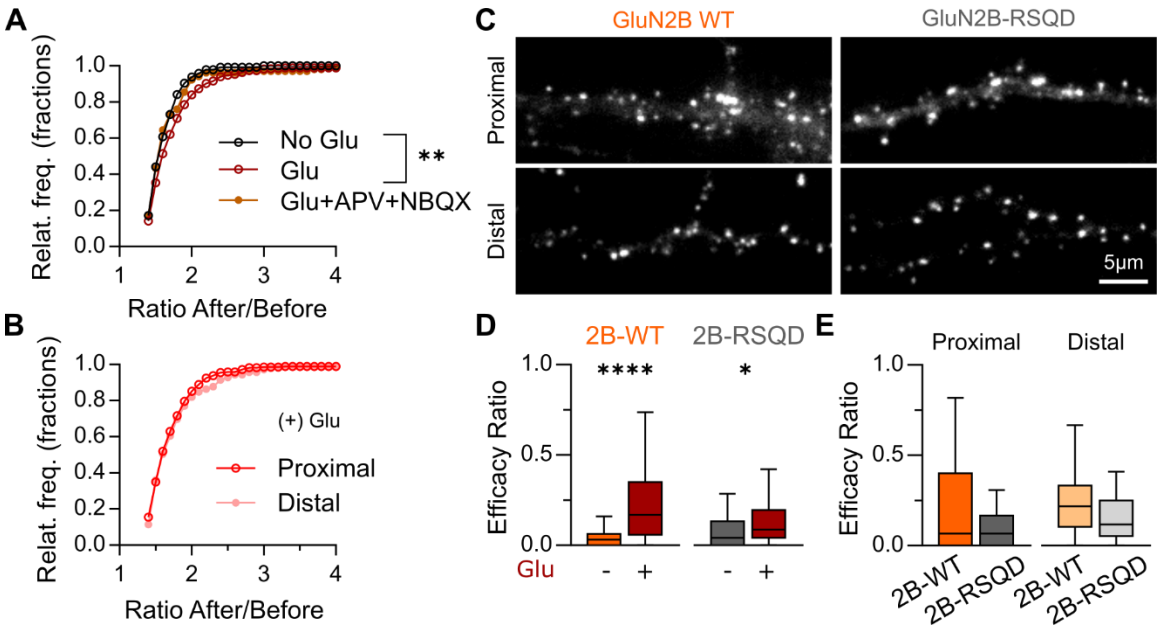

Fig. S4. The nano-organization of GluN2B-NMDAR differentially impacts synaptic potentiation capacities. (*A*) Relative frequency distributions (Relat. Freq.) of after/before SEP-GluA1 fluorescence mean intensity ratio at potentiated spines 20 min after uncaging in no glutamate (*black*), caged glutamate (*red*) and caged glutamate plus APV and NBQX (*brown*) conditions. (*B*) Relative frequency distributions of after/before SEP-GluA1 fluorescence intensity ratio at potentiated spines 20 min after uncaging at proximal (*dark color*) and distal (*light color*) dendritic segments in caged glutamate conditions. (*C*) Representative epifluorescent images of wild-type mCherry-GluN2B (*GluN2B WT; right panels*) and the CaMKII binding-deficient mutant mCherry-GluN2B-RSQD experiments (*GluN2B-RSQD; left panels*) at proximal (*top*) and distal (*bottom*) dendritic segments. (*D*) Efficacy ratio at spines from wild-type mCherry-GluN2B (*2B-WT; orange*) and mCherry-GluN2B-RSQD (*2B-RSQD; gray*) co-transfected neurons in no glutamate or caged-glutamate conditions (*red*). (*E*) Efficacy ratio at spines from wild-type mCherry-GluN2B (*2B-WT; orange*) and mCherry-GluN2B-RSQD (*2B-RSQD; gray*) co-transfected neurons in located in proximal (*dark colors*) and distal (*light colors*) dendritic segments in

glutamate conditions. Data are represented as box and whisker plots: line at median, IQR box, whiskers minimum and maximum values. * P ≤ 0.05; **** P ≤ 0.0001; no symbol *P* > 0.05. For statistical details refer to *SI Appendix, Table S1*.

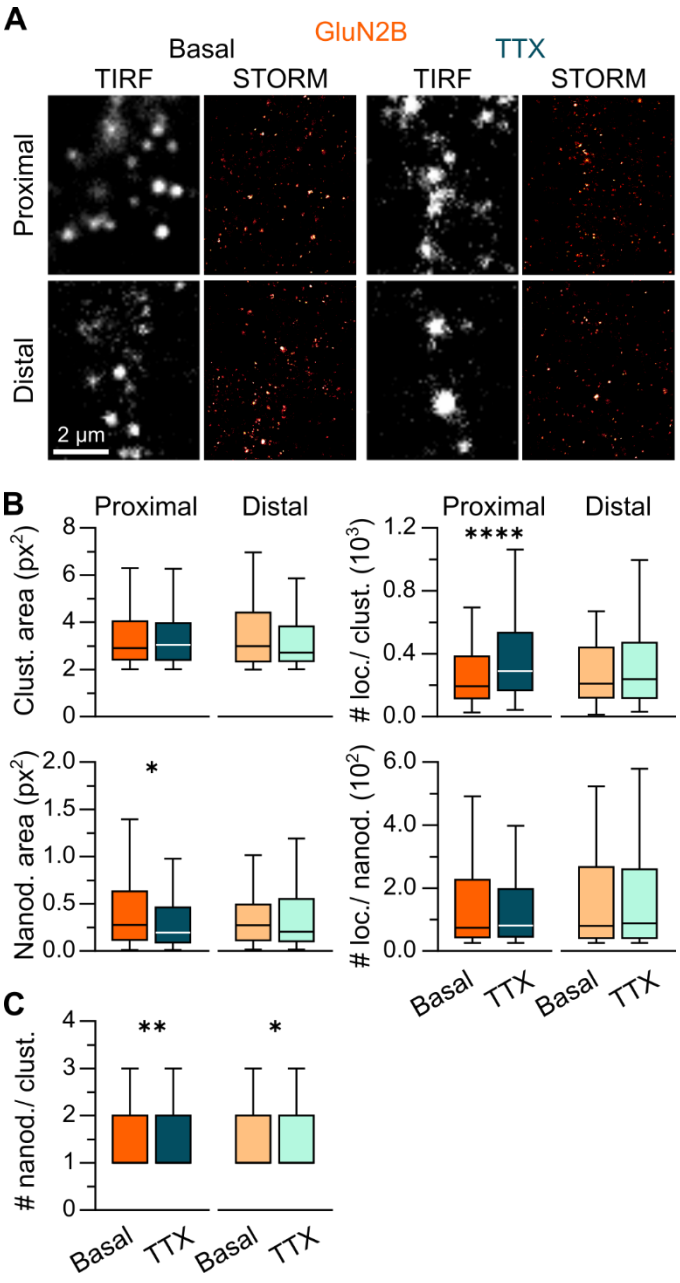

Fig. S5. Neuronal activity regulates the nanoscale organization of GluN2B-NMDAR at proximal locations. (*A*) Representative low resolution (TIRF) and super-resolved (dSTORM) images of GluN2B-NMDAR at proximal (*top panels*) and distal (*bottom panels*) locations in buffer (Basal; *left*) or after incubation with tetrodotoxin (TTX; *right*). *(B)* Cluster areas (Clust. area; *top left*), number of localizations per cluster (# loc./ clust.; *top right*), nanodomain areas (Nanod. area;

bottom left) and number of localizations per nanodomain (# loc./ nanod.; *bottom right*) of GluN2B-NMDAR (*orange*) at proximal (*dark colors*) and distal (*light colors*) locations in basal or TTX (*cyan*) conditions. *(C)* Number of nanodomains per cluster (#nanod./ clust.) of GluN2B-NMDAR (*orange*) at proximal (*dark colors*) and distal (*light colors*) locations in basal or TTX (*cyan*) conditions. Data are represented as box and whisker plots: line at median, IQR box, whiskers minimum and maximum values. * $P \leq 0.05$; ** $P \leq 0.01$; **** $P \leq 0.0001$; no symbol $P > 0.05$. For statistical details refer to *SI Appendix, Table S1*.

SI References

1. L. Bard, *et al.*, Dynamic and specific interaction between synaptic NR2-NMDA receptor and PDZ proteins. *Proc. Natl. Acad. Sci.* **107**, 19561–19566 (2010).
2. S. Kaech, G. Banker, Culturing hippocampal neurons. *Nat. Protoc.* **1**, 2406–2415 (2006).
3. B. Kellermayer, *et al.*, Differential Nanoscale Topography and Functional Role of GluN2-NMDA Receptor Subtypes at Glutamatergic Synapses. *Neuron* **100**, 106-119.e7 (2018).
4. K. She, J. K. Rose, A. M. Craig, Differential stimulus-dependent synaptic recruitment of CaMKIIα by intracellular determinants of GluN2B. *Mol. Cell. Neurosci.* **51**, 68–78 (2012).
5. M. M. Vieira, *et al.*, Multiple domains in the C-terminus of NMDA receptor GluN2B subunit contribute to neuronal death following in vitro ischemia. *Neurobiol. Dis.* **89**, 223–234 (2016).
6. J. Jézéquel, *et al.*, Dynamic disorganization of synaptic NMDA receptors triggered by autoantibodies from psychotic patients. *Nat. Commun.* **8**, 1791 (2017).
7. M. Heilemann, *et al.*, Subdiffraction-Resolution Fluorescence Imaging with Conventional Fluorescent Probes. *Angew. Chemie Int. Ed.* **47**, 6172–6176 (2008).
8. S. van de Linde, M. Sauer, M. Heilemann, Subdiffraction-resolution fluorescence imaging of proteins in the mitochondrial inner membrane with photoswitchable fluorophores. *J. Struct. Biol.* **164**, 250–254 (2008).
9. A. Kechkar, D. Nair, M. Heilemann, D. Choquet, J.-B. Sibarita, Real-Time Analysis and Visualization for Single-Molecule Based Super-Resolution Microscopy. *PLoS One* **8**, e62918 (2013).
10. A. Beghin, *et al.*, Localization-based super-resolution imaging meets high-content screening. *Nat. Methods* **14**, 1184–1190 (2017).
11. A. Dosemeci, T. S. Reese, J. Petersen, J. H. Tao-Cheng, A novel particulate form of Ca(2+)/calmodulin-dependent [correction of Ca(2+)/CaMKII-dependent] protein kinase II in neurons. *J. Neurosci.* **20**, 3076–84 (2000).

12. J. B. Myers, *et al.*, The CaMKII holoenzyme structure in activation-competent conformations. *Nat. Commun.* **8** (2017).
13. A. G. Shanbhag, Utilization of Information Measure as a Means of Image Thresholding. *CVGIP Graph. Model. Image Process.* **56**, 414–419 (1994).

Table S1. Statistical details

Figure	Parameter	Condition	Statistical test	Median ± IQR (non parametric data) Mean ± SEM (parametric data)	n	number of cells	independent experiments	P value
1D	Clust. Area	GluN2A - proximal	Mann Whitney test	4.11 ± 2.49	334 clusters	6	6	0.0513
		GluN2A - distal		1.90 ± 1.40	16 clusters			
		GluN2B - proximal		2.16 ± 1.97	583 clusters	8	7	0.0043
		GluN2B - distal		1.88 ± 1.22	114 clusters			
	# loc./ clust.	GluN2A - proximal	Mann Whitney test	297.5 ± 515.5	334 clusters	6	6	0.0993
		GluN2A - distal		559.5 ± 594.7	16 clusters			
		GluN2B - proximal		441 ± 624	583 clusters	8	7	<0.0001
		GluN2B - distal		688.5 ± 870.7	114 clusters			
	Local dens.	GluN2B - proximal	Mann Whitney test	178.7 ± 221.4	583 clusters	8	7	<0.0001
		GluN2B - distal		333.3 ± 393.6	114 clusters			
1E	Nanod. Area	GluN2A - proximal	Mann Whitney test	0.13 ± 0.20	556 nanodomains	6	6	0.2405
		GluN2A - distal		0.21 ± 0.42	19 nanodomains			
		GluN2B - proximal	Mann Whitney test	0.13 ± 0.33	877 nanodomains	8	7	<0.0001
		GluN2B - distal		0.06 ± 0.17	139 nanodomains			
	# loc./ nanod.	GluN2A - proximal	Mann Whitney test	77 ± 132.8	556 nanodomains	6	6	0.0113
		GluN2A - distal		182 ± 360	19 nanodomains			
		GluN2B - proximal	Mann Whitney test	101 ± 237	877 nanodomains	8	7	0.0353
		GluN2B - distal		120 ± 347	139 nanodomains			
	Local dens.	GluN2B - proximal	Mann Whitney test	899.3 ± 700.8	877 nanodomains	8	7	<0.0001
		GluN2B - distal		2693 ± 1879	139 nanodomains			
1G	Diff. coeff.	YFP-2A - proximal	Mann Whitney test	0.0009 ± 0.012	467 trajectories	19	7	0.0959
		YFP-2A - distal		0.0007 ± 0.0099	559 trajectories	18		
		YFP-2B - proximal	Mann Whitney test	0.0013 ± 0.0098	1172 trajectories	26	7	0.0025
		YFP-2B - distal		0.0008 ± 0.0059	1298 trajectories	25		
	Syn. resid. time	YFP-2A - proximal	Mann Whitney test	2.9 ± 6.9	467 trajectories	19	7	0.1892
		YFP-2A - distal		4.3 ± 12.3	559 trajectories	18		
		YFP-2B - proximal	Mann Whitney test	2.9 ± 10.4	1172 trajectories	26	7	0.0195
		YFP-2B - distal		5.1 ± 13.9	1298 trajectories	25		
2B	Int. Dens.	CaMKII - proximal	Paired t test	1 ± 0	24 cells	24	3	0.0001
		CaMKII - distal		0.73 ± 0.06	24 cells			
2D	Local density Clust.	CaMKII - proximal	Mann Whitney test	274.5 ± 393.2	193 clusters	5	4	<0.0001
		CaMKII - distal		94.57 ± 93.58	86 clusters			
2F	Local density Clust.	YFP-2B - proximal	Mann Whitney test	310 ± 324.2	374 clusters	7	4	0.0074
		-RSQD - proximal		368 ± 415.7	358 clusters	6	4	
		YFP-2B - distal	Mann Whitney test	382 ± 366.6	141 clusters	7	4	0.1973
		-RSQD - distal		461.9 ± 378.4	148 clusters	6	4	
	Local density Nanod.	YFP-2B - proximal	Mann Whitney test	1087 ± 654.1	598 nanodomains	7	4	<0.0001
		-RSQD - proximal		1523 ± 1010.1	609 nanodomains	6	4	
		YFP-2B - distal	Mann Whitney test	1196 ± 520.2	292 nanodomains	7	4	0.0315
		-RSQD - distal		1246 ± 423	339 nanodomains	6	4	
2G	Diff. coeff.	YFP-2B - proximal	Mann Whitney test	0.0013 ± 0.0098	1172 trajectories	26	7	<0.0001
		-RSQD - proximal		0.0005 ± 0.0059	851 trajectories	24		
		YFP-2B - distal	Mann Whitney test	0.0008 ± 0.0059	1298 trajectories	25	7	0.0128
		-RSQD - distal		0.0004 ± 0.0089	908 trajectories	24		
	Syn. Resid. Time	YFP-2B - proximal	Mann Whitney test	2.9 ± 10.4	1172 trajectories	26	7	0.002
		-RSQD - proximal		5.8 ± 14.3	851 trajectories	24		
		YFP-2B - distal	Mann Whitney test	5.1 ± 13.9	1298 trajectories	25	7	0.6676
		-RSQD - distal		5.6 ± 15.4	908 trajectories	24		
2I	Local density Clust.	TAT-NS	Mann Whitney test	186.7 ± 115.7	44 clusters	8	4	<0.0001
		AIP		503.5 ± 523.2	46 clusters	9	4	
	Local density Nanod.	TAT-NS	Mann Whitney test	786.1 ± 667.7	133 nanodomains	8	4	<0.0001
		AIP		1601 ± 1044	177 nanodomains	9	4	
3B	Efficacy Ratio	(-) Glu	Kruskal-Wallis test	0.034 ± 0.159	33 cells	33	6	<0.0001
		(+) Glu		0.190 ± 0.400	42 cells	42	6	
		(+) Glu, AP5, NBQX		0.091 ± 0.216	33 cells	15	3	
3C	Efficacy Ratio	(-) Glu - proximal	Mann Whitney test	0.000 ± 0.197	33 cells	33	6	0.0007
		(+) Glu - proximal		0.053 ± 0.127	42 cells	42	6	
		(-) Glu - proximal	Mann Whitney test	0.192 ± 0.565	33 cells	33	6	0.0005
		(+) Glu - proximal		0.210 ± 0.325	42 cells	42	6	
3E	Ratio After/Before	GluN2B - proximal	Kolmogorov-Smirnov test	1.605 ± 0.305	38 cells	141	8	<0.0001
		-RSQD - proximal		1.474 ± 0.152	39 cells	79	8	
		GluN2B - distal	Kolmogorov-Smirnov test	1.657 ± 0.422	38 cells	116	8	0.0076
		-RSQD - distal		1.570 ± 0.238	39 cells	90	8	
4B	Local density Clust.	Basal - proximal	Mann Whitney test	57.96 ± 68.26	246 clusters	22	4	<0.0001
		TTX - proximal		90.42 ± 89.79	190 clusters	23	4	
		Basal - distal	Mann Whitney test	64.34 ± 93.81	118 clusters	22	4	0.4097
		TTX - distal		78.62 ± 113.48	125clusters	23	4	
	Local density Nanod.	Basal - proximal	Mann Whitney test	357.5 ± 347.1	237 nanodomains	22	4	0.0001
		TTX - proximal		453.5 ± 384.6	256 nanodomains	23	4	
		Basal - distal	Mann Whitney test	433.2 ± 452.2	118 nanodomains	22	4	0.7624
		TTX - distal		446.2 ± 317.9	140 nanodomains	23	4	

Supplementary Figures

Figure	Parameter	Condition	Statistical test	Median ± IQR (non parametric data) Mean ± SEM (parametric data)	n	number of cells	independent experiments	P value
S1A	Homer-GFP area	proximal	Paired t test	62.07 ± 5.36	15 cells	15	6	0.031
		distal		43.67 ± 5.01				
S1B	# clust. / µm	GluN2A - proximal	Paired t test	1.95 ± 0.35	4 cells	4	4	0.2375
		GluN2A - distal		1.30 ± 0.61				
		GluN2B - proximal	Paired t test	2.20 ± 0.42	5 cells	5	5	0.1622
		GluN2B - distal		1.35 ± 0.35				
S1D	Local dens. Clust.	GluN2A - proximal	Mann Whitney test	98.34 ± 155.49	334 clusters	6	6	0.003
		GluN2A - distal		318.2 ± 400.8	16 clusters			
	Local dens. Nanod.	GluN2A - proximal	Mann Whitney test	681.6 ± 784.7	556 nanodomains	6	6	0.0067
		GluN2A - distal		1391 ± 1195.8	19 nanodomains			
S1E	# nanod./ clust.	GluN2A - proximal	Mann Whitney test	2 ± 2	262 clusters	6	6	0.0337
		GluN2A - distal		1 ± 1	14 clusters			
		GluN2B - proximal	Mann Whitney test	1 ± 1	435 clusters	8	7	0.41
		GluN2B - distal		1 ± 1	83 clusters			
S2B	Clust. Area	CaMKII - proximal	Mann Whitney test	1.40 ± 1.01	193 clusters	5	4	0.9725
		CaMKII - distal		1.44 ± 0.93	86 clusters			
	# loc./ clust.	CaMKII - proximal	Mann Whitney test	397 ± 841	193 clusters	5	4	<0.0001
		CaMKII - distal		141.5 ± 164.5	86 clusters			
S2D	Homer-DsRD area	YFP-2B - proximal	Paired t test	93.35 ± 9.2	13 cells	13	5	0.0056
		YFP-2B - distal		49.58 ± 7.91	13 cells			
		-RSQD - proximal	Paired t test	108.9 ± 13.3	13 cells	13	5	0.0014
		-RSQD - distal		44.44 ± 6.87	13 cells			
S2F	Clust. Area	YFP-2B - proximal	Mann Whitney test	2.02 ± 1.32	374 clusters	7	4	0.1706
		-RSQD - proximal		2.15 ± 1.79	358 clusters	6	4	
		YFP-2B - distal	Mann Whitney test	2.46 ± 2.33	141 clusters	7	4	0.6558
		-RSQD - distal		2.60 ± 2.78	148 clusters	6	4	
	# loc./ clust.	YFP-2B - proximal	Mann Whitney test	675.5 ± 892.2	374 clusters	7	4	0.002
		-RSQD - proximal		833 ± 1327.5	358 clusters	6	4	
		YFP-2B - distal	Mann Whitney test	1067 ± 1530	141 clusters	7	4	0.1665
		-RSQD - distal		1143 ± 1884.7	148 clusters	6	4	
	Nanod. Area	YFP-2B - proximal	Mann Whitney test	0.16 ± 0.39	598 nanodomains	7	4	0.0001
		-RSQD - proximal		0.11 ± 0.33	609 nanodomains	6	4	
		YFP-2B - distal	Mann Whitney test	0.15 ± 0.52	292 nanodomains	7	4	0.3004
		-RSQD - distal		0.15 ± 0.39	339 nanodomains	6	4	
	# loc./ nanod.	YFP-2B - proximal	Mann Whitney test	156 ± 406.6	598 nanodomains	7	4	0.2614
		-RSQD - proximal		129 ± 410.5	609 nanodomains	6	4	
		YFP-2B - distal	Mann Whitney test	163 ± 495.3	292 nanodomains	7	4	0.5208
		-RSQD - distal		153 ± 397	339 nanodomains	6	4	
S2G	# nanod./ clust.	YFP-2B - proximal	Mann Whitney test	1 ± 1	335 clusters	7	4	0.1649
		-RSQD - proximal		2 ± 1	308 clusters	6	4	
		YFP-2B - distal	Mann Whitney test	2 ± 2	129 clusters	7	4	0.4955
		-RSQD - distal		2 ± 2	138 clusters	6	4	
S2H	Surface Explored	YFP-2B - proximal	Mann Whitney test	0.0003 ± 0.0009	1172 trajectories	26	7	0.0365
		-RSQD - proximal		0.0002 ± 0.000052	851 trajectories	24		
		YFP-2B - distal	Mann Whitney test	0.0002 ± 0.00074	1298 trajectories	25	7	0.0662
		-RSQD - distal		0.0001 ± 0.000076	908 trajectories	24		
S3B	Clust. area	GluN2A - TAT-NS	Mann Whitney test	3.3 ± 1.74	86 clusters	9	3	0.7158
		GluN2A - AIP		3.18 ± 1.90	56 clusters	9		
		GluN2B - TAT-NS	Mann Whitney test	2.99 ± 2.37	44 clusters	8	4	0.2755
		GluN2B - AIP		2.62 ± 1.50	46 clusters	9		
	# loc./ clust.	GluN2A - TAT-NS	Mann Whitney test	1643 ± 1353.7	86 clusters	9	3	0.0221
		GluN2A - AIP		2022 ± 1430	56 clusters	9		
		GluN2B - TAT-NS	Mann Whitney test	665.5 ± 855.7	44 clusters	8	4	<0.0001
		GluN2B - AIP		1499 ± 1402	46 clusters	9		
	Nanod. Area	GluN2A - TAT-NS	Mann Whitney test	0.11 ± 0.15	389 nanodomains	9	3	0.145
		GluN2A - AIP		0.09 ± 0.14	279 nanodomains	9		
		GluN2B - TAT-NS	Mann Whitney test	0.13 ± 0.24	113 nanodomains	8	4	0.0073
		GluN2B - AIP		0.09 ± 0.21	177 nanodomains	9		
	# loc./ nanod.	GluN2A - TAT-NS	Mann Whitney test	154 ± 256	389 nanodomains	9	3	0.6429
		GluN2A - AIP		167 ± 282	279 nanodomains	9		
		GluN2B - TAT-NS	Mann Whitney test	110 ± 186	113 nanodomains	8	4	0.035
		GluN2B - AIP		137 ± 318	177 nanodomains	9		
S3C	# nanod./ clust.	GluN2A - TAT-NS	Mann Whitney test	4 ± 3	85 clusters	9	3	0.1451
		GluN2A - AIP		5 ± 3	56 clusters	9		
		GluN2B - TAT-NS	Mann Whitney test	3 ± 2	43 clusters	8	4	0.1025
		GluN2B - AIP		4 ± 4	45 clusters	9		
S3D	Local dens. Clust.	GluN2A - TAT-NS	Mann Whitney test	471.5 ± 401.1	86 clusters	9	3	0.0173
		GluN2A - AIP		575.2 ± 376.6	56 clusters	9		
	Local dens. Nanod.	GluN2A - TAT-NS	Mann Whitney test	1405 ± 997	389 nanodomains	9	3	<0.0001
		GluN2A - AIP		1796 ± 832	279 nanodomains	9		
S4A	After/Before Ratio	(-) Glu	Kruskal-Wallis test	1.577 ± 0.286	145 spines	33	6	0.0069
		(+) Glu		1.639 ± 0.406	430 spines	42	6	
		(+) Glu, AP5, NBQX		0.1588 ± 0.337	104 spines	15	3	
S4B	After/Before Ratio	(+) Glu - proximal	Kolmogorov-Smirnov test	1.639 ± 0.386	289 spines	42	6	0.6852
		(+) Glu - distal		1.642 ± 0.421	139 spines	42	6	
S4D	Efficacy Ratio	(-) Glu - GluN2B	Mann Whitney test	0.032 ± 0.064	36 cells	36	8	<0.0001
		(+) Glu - GluN2B		0.1682 ± 0.291	38 cells	38	8	
		(-) Glu - RSQD	Mann Whitney test	0.041 ± 0.1323	36 cells	36	8	0.0160
		(+) Glu - RSQD		0.087 ± 0.1544	38 cells	38	8	
S4E	Efficacy Ratio	GluN2B - proximal	Mann Whitney test	0.067 ± 0.400	38 cells	38	8	0.2287
		-RSQD - proximal		0.067 ± 0.167	39 cells	39	8	
		GluN2B - distal	Mann Whitney test	0.218 ± 0.229	38 cells	38	8	0.0694
		-RSQD - distal		0.118 ± 0.197	39 cells	39	8	
	Clust. area	Basal - proximal	Mann Whitney test	2.908 ± 1.634	246 clusters	22	4	0.8018
		TTX - proximal		3.039 ± 1.565	190 clusters	23		
		Basal - distal	Mann Whitney test	2.986 ± 2.067	118 clusters	22	4	0.6085

		TTX - distal	[illegible]	2.721 ± 1.480	125 clusters	23	[illegible]	[illegible]
S5B	# loc./ clust.	Basal - proximal	Mann Whitney test	195.0 ± 266.5	246 clusters	22	4	<0.0001
		TTX - proximal		290.5 ± 365.5	190 clusters	23		
		Basal - distal	Mann Whitney test	211.5 ± 319.0	118 clusters	22	4	0.700
		TTX - distal		238.0 ± 352.5	125 clusters	23		
	Nanod. Area	Basal - proximal	Mann Whitney test	0.2755 ± 0.516	237 nanodomains	22	4	0.0104
		TTX - proximal		0.1964 ± 0.371	256 nanodomains	23		
		Basal - distal	Mann Whitney test	0.2721 ± 0.378	118 nanodomains	22	4	0.6445
		TTX - distal		0.2040 ± 0.447	125 nanodomains	23		
	# loc./ nanod.	Basal - proximal	Mann Whitney test	74.0 ± 183.5	237 nanodomains	22	4	0.8696
		TTX - proximal		80.5 ± 151.8	256 nanodomains	23		
		Basal - distal	Mann Whitney test	80.0 ± 226.6	118 nanodomains	22	4	0.8127
		TTX - distal		88.0 ± 218.8	125 nanodomains	23		
S5C	# nanod./ clust.	Basal - proximal	Mann Whitney test	1 ± 1	246 clusters	22	4	0.0039
		TTX - proximal		1 ± 1	190 clusters	23		
		Basal - distal	Mann Whitney test	1 ± 1	118 clusters	22	4	0.0381
		TTX - distal		1 ± 1	125 clusters	23		